

The structure of 2D charge transfer salts formed by TCNQ/alkali metal coadsorption on Ag(111)

P.J. Blowey^{a,b}, L.A. Rochford^c, D.A. Duncan^b, P.T.P. Ryan^{b,d}, D.A. Warr^e, T.-L. Lee^b, G. Costantini^e, D.P. Woodruff^{a,*}

^a Physics Department, University of Warwick, Coventry CV4 7AL, UK

^b Diamond Light Source, Harwell Science and Innovation Campus, Didcot, OX11 0DE, UK

^c Chemistry Department, University of Birmingham, University Road, Birmingham B15 2TT, UK

^d Department of Materials, Imperial College, London SW7 2AZ, UK

^e Chemistry Department, University of Warwick, Coventry CV4 7AL, UK

ARTICLE INFO

Keywords:

Surface structure
Alkali adsorption
TCNQ
Charge transfer
STM
NIXSW

ABSTRACT

The structure of coadsorption phases formed on Ag(111) by TCNQ (7,7,8,8-tetracyanoquinodimethane) with Cs are compared with previously reported coadsorption phases formed with K, following investigation by scanning tunnelling microscopy (STM), low energy electron diffraction, soft X-ray photoelectrons spectroscopy and normal incidence X-ray standing waves (NIXSW). For each alkali we identify two ordered phases, one with an alkali: TCNQ stoichiometry of 1:1 and the other 2:1. STM images show the molecular organisation is the same for Cs and K, although only the K₂TCNQ phase is commensurate with the substrate. A previously-published detailed structure determination of the K₂TCNQ phase, complemented by density function theory calculations that identify bonding strengths, showed that the binding within the layer is much stronger than that of the layer to the substrate. Insensitivity to commensuration is thus to be expected. The situation for KTCNQ and CsTCNQ is less clear; these ordered incommensurate overlayers clearly have strong intralayer bonding, but the relative strength of the average overlayer-substrate bonding is unknown. NIXSW data show that the alkalis in these phases occupy adsorption sites far more distant from the substrate than the TCNQ molecules when compared to the near coplanar alkali-TCNQ geometry of K₂TCNQ and Cs₂TCNQ. Ultraviolet photoelectron spectra show increasing bonding shifts of TCNQ orbital states with alkali coverage.

1. Introduction

The important role of metal-organic interfaces in determining the electronic properties of devices based on organic semiconductors has led to a number of surface science studies of related model systems. One molecule of particular interest is 7,7,8,8-tetracyanoquinodimethane (TCNQ), which is a strong electron acceptor capable of forming highly conducting charge transfer salts in combination with suitable electron donor molecules. As such there have been a number of studies of TCNQ adsorption on coinage metal (111) surfaces. (e.g. [1–12]). Coadsorption of TCNQ with alkali metals offers a way of producing 2D salt layers, as well as a way of modifying the surface work function and thus the electronic energy alignment at the metal-organic interface [13]. Knowledge of the structure of these salts is a prerequisite to understanding their properties. To explore this idea we report here on the full characterisation of the structures formed by coadsorption of TCNQ with Cs and with K on the Ag(111) surface, including quantitative structural

data on the adsorption heights using the technique of normal incidence X-ray standing waves (NIXSW) [14]. The results of our investigation of TCNQ/K coadsorption phases on this surface, identifying two distinct phases of different TCNQ/K stoichiometry, have already been reported in detail [15–17]; these include a particularly complete study of a phase of K₂TCNQ stoichiometry, which is commensurate with the substrate and therefore accessible to density functional theory (DFT) calculations. These calculations, aided by the benchmark NIXSW data, gave insight into the nature of the bonding within the overlayer and to the underlying Ag(111) [16]. For coadsorption of Cs with TCNQ we have identified no commensurate coadsorption phases accessible to DFT slab calculations, but find two ordered incommensurate Cs/TCNQ phases that appear to have similar organisation of the coadsorbed species to the two K/TCNQ phases. This provides an interesting base for comparison of the effect of the different alkali metal ion on the unit mesh dimensions and the height of the molecules above the surface, as determined by NIXSW. The fact that similar alkali/TCNQ layers may

* Corresponding author.

<https://doi.org/10.1016/j.susc.2020.121687>

Received 10 April 2020; Received in revised form 7 July 2020; Accepted 9 July 2020

Available online 10 July 2020

0039-6028/ © 2020 Elsevier B.V. All rights reserved.

readily form without substrate commensurability, apparently insensitive to the lateral corrugation of the overlayer-substrate potential, might be explained by the fact that all of these layers are actually 2D charge transfer salts with strong bonding within the layer and weaker bonding to the underlying surface. We recently demonstrated this very precisely in the specific case of the commensurate Ag(111)-K₂TCNQ system [16]. Here we present the experimental characterisation of all four phases, providing the basis for a possible generalisation of this phenomenon.

2. Experimental details

Identification and characterisation of the adsorption phases was conducted in a UHV chamber at the University of Warwick equipped with facilities for both room temperature scanning tunnelling microscopy (STM), low-current (and hence low radiation damage) micro-channel plate low energy electron diffraction (MCP-LEED) and ultra-violet photoelectron spectroscopy (UPS). Further characterisation and quantitative structural data were obtained using synchrotron radiation X-ray photoelectron spectroscopy (SXPS) and normal incidence X-ray standing wave (NIXSW), performed in the UHV end-station installed on beamline I09 of the Diamond Light Source. MCP-LEED at both locations provided a crucial cross-reference for the preparation of equivalent adsorbed layers under similar conditions. The single crystal Ag(111) samples (Surface Preparation Laboratory, The Netherlands and MaTecK, Germany) were cleaned *in situ* using cycles of sputtering with 1 keV Ar⁺ ions for 30 minutes followed by annealing to ~500 °C for another 30 minutes. STM images, recorded in constant current mode using electrochemically etched polycrystalline tungsten tips, were plane corrected and flattened using the open source image-processing software Gwyddion [18].

NIXSW measurements to monitor the X-ray absorption at the C and N atoms of TCNQ, as well as at the co-adsorbed K and Cs atoms, were achieved by recording the intensity of the C 1s, N 1s, K 2p and Cs 3d photoelectron spectra, collected using a VG Scienta EW4000 HAXPES hemispherical electron analyser mounted at 90° to the incident photon beam, while sweeping the photon energy through the (111) Bragg condition at near-normal incidence to the surface. Both the high-resolution SXP spectra (measured using ‘soft’ X-rays at photon energies of ~400–900 eV, chosen to yield low photoelectron kinetic energies and thus higher spectral resolution and higher photoionisation cross-section) and the ‘HAXPE’ spectra recorded in NIXSW experiments (photoemission spectra at the ‘harder’ X-ray energies corresponding to the Bragg scattering condition at ~2630 eV) were fitted using the CasaXPS software package to allow chemical-state specific NIXSW data to be extracted. Fitting of the NIXSW absorption profiles to extract the structural parameters included taking account of the non-dipolar effects on the angular dependence of the photoemission, using values for the backward-forward asymmetry parameter *Q* [19], obtained from theoretical angular distribution parameters [20].

TCNQ powder (98% pure; Sigma Aldrich) was triply purified by thermal gradient sublimation and thoroughly degassed before being deposited onto the Ag(111) substrate held at room temperature, by using an organic molecular beam epitaxy source operated at a nominal temperature of 120 °C. Cs and K were deposited by resistive heating of SAES dispenser sources, previously calibrated by XPS. Coadsorption phases were prepared by first depositing a nominal saturation coverage of TCNQ and annealing the sample to 280 °C to produce the ordered commensurate $\begin{pmatrix} 2 & 5 \\ -8 & -2 \end{pmatrix}$ sub-monolayer TCNQ adsorption phase [8], followed by sequential dosing of the alkali atoms (with the sample at room temperature) and subsequent heating to 200 °C.

3. Characterisation of coadsorption phases

Details of the identification and properties of K/TCNQ coadsorption

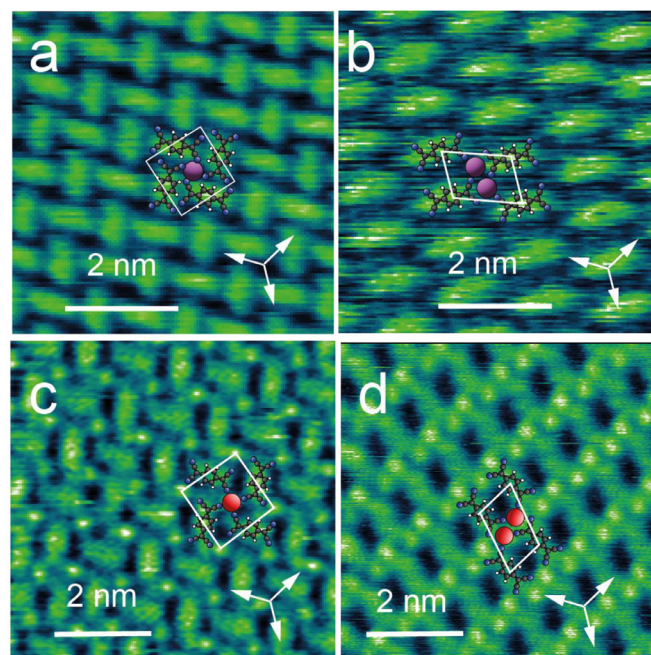


Fig. 1. STM images of the (a) KTCNQ ‘windmill’ (b) K₂TCNQ ‘head-to-tail’. (c) CsTCNQ ‘windmill’ and (d) Cs₂TCNQ ‘head-to-tail’ coadsorption phases on Ag (111), with superimposed structural models and unit meshes. The white arrows identify the <110> surface azimuths. Scan parameters: (a) 0.1 V, 175 pA (b) -0.6 V, 100 pA, (c) and (d) -0.9 V, 300 pA.

phases have been published elsewhere. Briefly, an incommensurate $\begin{pmatrix} 4.28 & 4.93 \\ -3.22 & 2.09 \end{pmatrix}$ phase was identified by LEED and STM and details of this phase and the associated NIXSW data were reported [15], as have similar data and a complete analysis of the structure and electronic properties of a commensurate $\begin{pmatrix} 3 & 0 \\ 1 & 5 \end{pmatrix}$ phase, aided by dispersion-corrected density function theory (DFT) calculations [16]. The stoichiometries of these two phases have been identified on the basis of SXP spectra as KTCNQ and K₂TCNQ, respectively. A low energy electron microscopy (LEEM) investigation of the development of these two phases also identified two additional, but apparently metastable, phases [17]. STM images from the KTCNQ and K₂TCNQ phases are shown in Fig. 1(a) and Fig. 1(b), with superimposed structural models. For the KTCNQ phase, the STM image shows distinct features having the expected shape and approximate size for TCNQ molecules, arranged like the four vanes of a windmill; for convenience we refer to this structure hereafter as the ‘windmill phase’ (Fig. 1a). As discussed in ref [15], this type of arrangement of TCNQ molecules surrounding a single metal atom has been seen in a number of other TCNQ coadsorption systems, so we infer that in this system, too, K atoms are surrounded by four TCNQ molecules, although the STM images show no consistent features that could be readily assigned to the location of the K atoms (see also below). This juxtaposition of K atoms and TCNQ molecules is also found in the bulk crystalline phase of KTCNQ [21]. The arrangement of the molecules differs in the K₂TCNQ phase (Fig. 1b), which we refer to as the ‘head-to-tail’ phase, for which a full quantitative structure determination has been reported [16].

Similar preparation procedures led to the identification of three distinct long-range ordered Cs/TCNQ coadsorption phases with increasing concentrations of Cs. At low Cs concentrations an extremely complex phase with a large unit mesh (approximate dimensions 34.8 Å × 39.0 Å with an included angle of 97°) was observed by STM, with a LEED pattern involving very large numbers of near-overlapping diffracted beams. STM images and a LEED pattern of this phase are shown in Fig. S1 of the ESI. Based on the STM images, it seems that the unit

mesh may contain as many as 16 molecules and an unknown number of Cs atoms. No attempt has been made to try to construct a meaningful model of this structure and no SXPS or NIXSW was recorded from preparations of this phase. At higher Cs concentrations, however, two smaller unit mesh structures were found with STM (Fig. 1(c) and Fig. 1(d)) and LEED (see Fig. S2 of the ESI). Both of these phases are incommensurate with the substrate with unit meshes described by the matrices $\begin{pmatrix} 4.51 & 5.07 \\ -3.44 & 1.83 \end{pmatrix}$ and $\begin{pmatrix} 3.22 & 0 \\ 0.73 & 4.68 \end{pmatrix}$. Although the detailed appearance of the STM images from these Cs/TCNQ phases differ from those of K/TCNQ, they have molecular arrangements that can also be described as ‘windmill’ and ‘head-to-tail’, respectively. Notice that in these images essentially circular bright features are present that can probably be attributed to Cs atoms, leading to estimated stoichiometries of CsTCNQ and Cs₂TCNQ, respectively. The locations of these bright circles relative to the TCNQ molecules correspond to the positions we believe K atoms adopt in the KTCNQ [15] and K₂TCNQ [16] phases. It is unclear why the alkali atoms should be clearly visible in the Cs/TCNQ images but not in the K/TCNQ images, but there are ample examples in the literature of both STM-visible e.g. [22,23] and STM-invisible adatoms, e.g. [15,24], in 2-dimensional metal-organic frameworks (2D-MOFs) on surfaces. One possible reason may be the exact operating conditions or the state of the tip. Notice that the image of the KTCNQ phase was recorded with positive sample bias, while the remainder used negative sample bias. Some images recorded from the KTCNQ phase with negative bias did show features attributable to the presence of the K atoms [15], but could not be reproduced reliably. No conditions were found that showed features attributable to K atoms in images of the K₂TCNQ phase, though the search of tunnelling parameters was not exhaustive. Of course, fundamentally, STM is a probe of the electronic properties of the near-surface region, not of the underlying atomic positions, so while there is no simple generic way of predicting the specific situations in which visibility and non-visibility should occur, the fact that such differences in behaviour occur is not particularly surprising. DFT simulations of the STM images from the commensurate K₂TCNQ phase are consistent with the failure to image the K atoms in this phase [16].

Clearly there are strong similarities in the structures of the K/TCNQ and Cs/TCNQ 2D-MOF phases, despite the fact that only one of them (K₂TCNQ) is commensurate with the underlying Ag(111) surface. Specifically, the arrangements of the TCNQ molecules relative to the alkali atoms are essentially equivalent and the sizes and shapes of the unit meshes are closely similar, although those involving Cs are slightly larger than those involving K. Specifically, expressed as multiples of the unit mesh of the underlying Ag(111) surface, the areas of KTCNQ and CsTCNQ phase unit meshes are 24.81 and 25.69, respectively (each containing two alkali atoms and two TCNQ molecules), while those of K₂TCNQ and Cs₂TCNQ are 14.00 and 15.07, respectively (each containing two alkali atoms and one TCNQ molecule). These areas, in nm², are also given in Fig. 2. The slightly larger unit mesh sizes of the Cs phases can probably be attributed to the larger atomic, or, more appropriately, ionic radius of Cs relative to that of K. Notice, incidentally, that one principal translation vector of both the K₂TCNQ and the Cs₂TCNQ head-to-tail phases is aligned along one of the $\langle 110 \rangle$ azimuthal directions of the primitive translation vectors of the substrate.

In addition to these comparisons of the lateral periodicity of the K-TCNQ and Cs-TCNQ 2D MOFs, our NIXSW results provide a comparison of the heights of the constituent atoms above the Ag(111) surface.

The NIXSW technique [14] exploits the X-ray standing wave formed by the interference of incident and scattered X-rays at a Bragg condition. By using core level photoemission to determine the X-ray absorption at atoms immersed in the standing wave as a function of photon energy one obtains a spectral profile characteristic of the height of the absorbing atoms above the Bragg scattering planes in an element- and chemical-state specific fashion. These data can be uniquely fitted by two structural parameters, the coherent fraction, f_{co} , and the

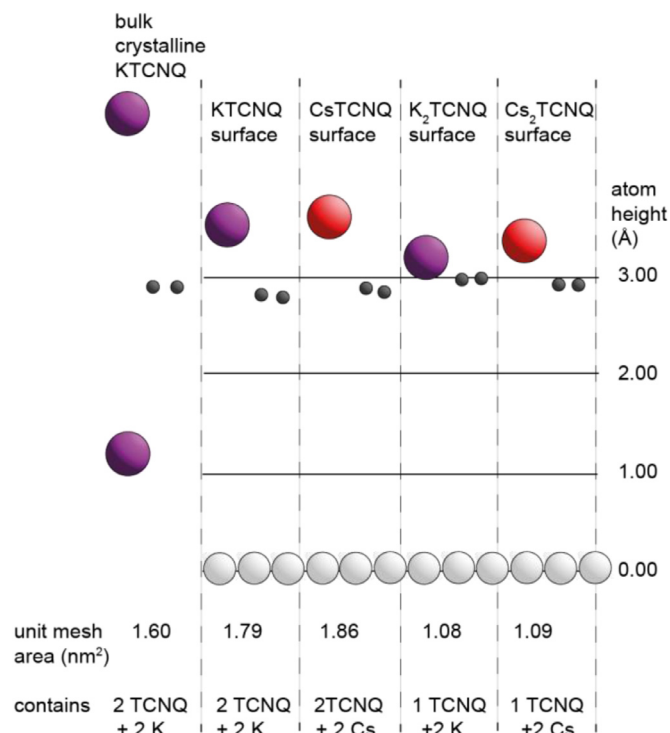


Fig. 2. Schematic representation of the relative heights of the K (purple), Cs (red) and CH and CC (black) atoms above the Ag(111) surface according to the NIXSW data of Table 1. Also shown are the relative heights of the alternating K and TCNQ layers in bulk crystalline KTCNQ; in this case the (arbitrary) absolute height of the C atoms is approximately aligned with those of the surface phases to aid comparison. Also shown are the unit mesh areas and number of alkali atoms and TCNQ molecules in each unit mesh. (For interpretation of the references to color in this figure legend, the reader is referred to the web version of this article.)

coherent position, p . The coherent fraction is commonly regarded as an order parameter, and for values of this parameter greater than ~ 0.8 , the associated value of the coherent position gives the height of the absorbing atoms, $D_{(111)}$, relative to the atomic scattering planes of the Bragg reflection. As the surface plane is parallel to the (111) Bragg scattering plane, $D_{(111)}$ is the height of the absorbing atom above the surface (disregarding any potential surface relaxations). However, much lower values of f_{co} indicate that there are likely to be two or more contributing heights, the measured coherent position being a weighted average of these different values. Values of these parameters, extracted from our NIXSW experiments, are listed in Table 1 for the K-TCNQ and Cs-TCNQ coadsorption phases. Notice that the C 1s XP spectra clearly

Table 1

NIXSW f and D values (the latter converted from coherent position p using $n = 1$) for the K/TCNQ and Cs /TCNQ coadsorption phases (error estimates, discussed in ref [15], are shown in parentheses in units of 0.01).

	KTCNQ windmill		K ₂ TCNQ head-to-tail	
	f_{co}	$D_{(111)}$ (Å)	f_{co}	$D_{(111)}$ (Å)
K	0.79(10)	3.56(5)	0.81(10)	3.29(7)
CH	1.00(10)	2.85(5)	0.86(10)	2.97(5)
CC	1.00(10)	2.79(5)	0.66(10)	2.99(5)
CN	0.91(10)	2.79(5)	0.56(10)	3.22(5)
N	0.41(10)	2.79(5)	0.55(12)	3.30(5)
	CsTCNQ windmill		Cs ₂ TCNQ head-to-tail	
	f_{co}	$D_{(111)}$ (Å)	f_{co}	$D_{(111)}$ (Å)
Cs	0.52(10)	3.64(5)	0.79(10)	3.40(5)
CH	1.01(10)	2.87(5)	0.90(10)	2.89(5)
CC	1.06(10)	2.83(5)	0.80(10)	2.89(5)
CN	0.96(10)	2.82(5)	0.67(10)	3.09(5)
N	0.79(10)	2.71(5)	0.41(10)	3.05(5)

show at least three clearly resolved chemically-shifted components (see Fig. S3) which are attributed to the C atoms bonded to H, those bonded only to carbon, and those bonded to N. NIXSW data extracted from these three components are identified as CH, CC and CN in the table.

Comparison of the $D_{(111)}$ values of the Cs phases (also represented in the schematic diagram of Fig. 2) reveals two clear patterns. Firstly, in the 1:1 alkali:TCNQ stoichiometry phases (the windmill phases) the alkali atom lies some 0.7–0.8 Å above the atoms within the TCNQ molecule, which is approximately planar and parallel to the surface. Secondly, in the 2:1 stoichiometry phases (the head-to-tail phases) the peripheral atoms of the TCNQ molecules are nearly coplanar with (only 0.01–0.35 Å below) the alkali atoms, while the central atoms (CH, CC) of the TCNQ lie ~ 0.14 –0.33 Å closer to the surface than the peripheral atoms. Inspection of the associated f values, however, shows that, with the possible exception of the CsTCNQ phase, the N atoms probably occupy sites with more than one height above the surface, which may indicate some twisting of the molecule. However, at least part of the reason for the reduced f values for the CN and N absorbers for K_2 TCNQ may be due to some co-occupation of KTCNQ domains which does occur during the surface preparation of the higher K coverage phase [25]; these are the atoms with the largest difference in $D_{(111)}$ values for these two phases. The coherent fraction for the Cs atoms in the CsTCNQ phase is also rather low, which also suggests a possible co-occupation of more than one height for this phase.

The strong similarity of the lateral periodicities, the relative atomic heights, and the molecular organisation within the surface unit meshes of the K/TCNQ and Cs/TCNQ phases clearly indicates that the detailed structures formed by the two alkalis are extremely similar. It is thus helpful to review the situation for the K/TCNQ phases, which have been reported individually but not previously compared in this way, and to attempt to generalise the results to the Cs/TCNQ phases. Our understanding of the K_2 TCNQ phase is most complete because this commensurate phase can be investigated by DFT calculations and the results of a comparison of the NIXSW measurements and the optimised DFT structure (with excellent agreement) provide a rather detailed and strongly supported structural model [16]. On the other hand, as the KTCNQ phase is incommensurate with the substrate, DFT calculations were not possible and so the model is less detailed [15]. However, it is very instructive to compare directly graphic models of the two structures, side views of which are displayed in Fig. 3.

There are two striking differences in the NIXSW structure parameter values for KTCNQ relative to those of the K_2 TCNQ phase: the heights of the K and TCNQ components, and the low f_{co} value for CN and N atoms. In both phases, the TCNQ molecules are evidently bonded through the cyano N atoms to the K^+ ions that sit high above the surface, while the central core of the molecule is slightly lower. However, the difference in

height between the K and the TCNQ is greater in the KTCNQ surface phase than in the K_2 TCNQ phase. Specifically, the K atoms are higher above the surface, and the molecules lower, in the KTCNQ phase. As described previously, the low f_{co} values of CN and N atoms in the KTCNQ phase have been rationalised [15] as a consequence of a twisting of the TCNQ molecules away from an ideal planar geometry parallel to the Ag(111) surface.

This twisted geometry is also a feature of the structure of the bulk KTCNQ crystalline phase [21] in which each K^+ ion has 8 TCNQ neighbours, 4 in the layer below, 4 in the layer above, with the molecules being arranged like windmill vanes around the central K^+ ion. This 3D phase comprises alternate layers of K^+ ions and TCNQ molecules with a spacing of 1.79 Å, which is more than twice the height difference (~ 0.76 Å) between K and TCNQ in the Ag(111)/KTCNQ phase (see Table 1 and Fig. 2). One effect that would contribute to the lower layer separation is that the unit mesh (the 2D projection of the unit cell) within the bulk crystal has dimensions $12.676 \text{ Å} \times 12.614 \text{ Å}$ (included angle 90°) whereas in the KTCNQ surface phase these dimensions are $13.7 \pm 0.4 \text{ Å} \times 13.0 \pm 0.4 \text{ Å}$ (included angle 88°); the unit mesh areas are compared in Fig. 2. This larger mesh should lead to a larger ‘hole’ in the TCNQ layers allowing the interlayer spacing to decrease, but this small size difference cannot alone account for the large difference in K-TCNQ layers spacing in the bulk and surface phases. However, another important difference is the impact of the large dipole moment perpendicular to the surface due to the separation of the K^+ and TCNQ $^-$ sheets, and the additional dipole moment due to interaction with the image charges in the conducting substrate. In the bulk crystal the alternation of layers leads to alternating dipoles, but there are no balancing opposite dipoles with a single layer of each component, so these dipolar interactions can be expected to significantly reduce the K^+ -TCNQ $^-$ layer spacing, relative to its value in bulk crystalline KTCNQ.

There appears to be no published structure determination of any bulk CsTCNQ crystalline phase with 1:1 stoichiometry, though Cs_2 TCNQ $_3$ has been reported [26]. For Rb, which lies between K and Cs in the periodic table, the 1:1 bulk crystal structure formed with TCNQ has the same space group as KTCNQ [27]. The NIXSW data for the Cs-TCNQ phases on Ag(111) show very similar differences between the structural parameters of the windmill and head-to-tail phases when compared to the K/TCNQ phases (Table 1). As a consequence, there seems no reason to believe that the structural arrangements of the K-induced and Cs-induced 2D-MOF phases differ significantly, implying that structural models similar to those shown in Fig. 3 should also describe rather well the CsTCNQ and Cs_2 TCNQ phases on Ag(111).

The fact that only one of the four surface phases is commensurate with the Ag(111) surface clearly implies that the bonding of the species within the overlayer is strong compared with the lateral (crystalline) corrugation of the overlayer-substrate bonding. Indeed, the detailed DFT analysis of the K_2 TCNQ phase [16] leads to the conclusion not only that the overlayer forms a 2D charge transfer salt with a high cohesive energy, but also that the bonding to the substrate is much weaker than in the absence of the coadsorbed alkali. Indeed, the calculated electron transfer to the TCNQ molecules is almost entirely from the coadsorbed K atoms rather than the Ag substrate. The similarity of the measured structural parameters for the Cs_2 TCNQ phase and for the K_2 TCNQ would lead one to assume that a similar balance of bonding strengths and charge transfer occurs in this phase. Less obvious is that this is necessarily true for the relative values of the intralayer bonding and the overlayer-substrate bonding, in the KTCNQ and CsTCNQ phases, in which the alkali atoms are much less embedded in the TCNQ layer. However, the fact that these phases also form well-ordered incommensurate overlayers does suggest that they also have strong intralayer bonding and weaker overlayer-substrate bonding.

While we may anticipate that similar alkali-TCNQ 2D charge transfer salts will occur on other substrates, the apparent insensitivity to the overlayer-substrate registry (notably the insensitivity to

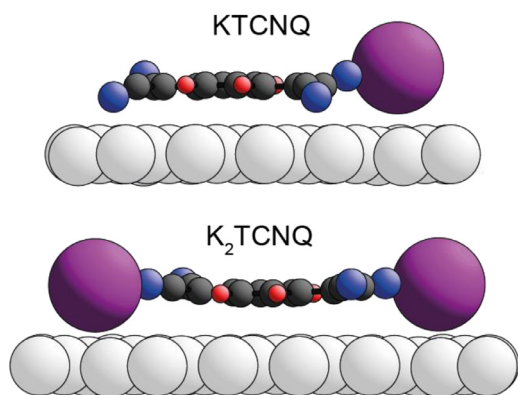


Fig. 3. Side views of the structures of the KTCNQ and K_2 TCNQ phases on Ag(111). For K_2 TCNQ, the structure is fully determined in ref [16] by a combination of STM, NIXSW and DFT calculations. For KTCNQ, the model is based only on the STM and NIXSW results [15].

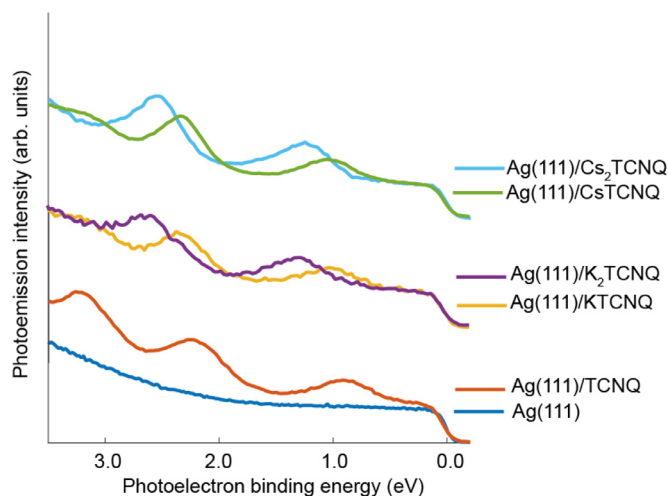


Fig. 4. UPS obtained from the K/TCNQ and Cs/TCNQ adsorption phases on Ag(111), and the clean Ag(111) substrate and from pure TCNQ on Ag(111). The ordinate intensity scale is arbitrary and the spectra are scaled and offset relative to each other for clarity. Measurements were obtained using the He-I α ($h\nu = 21.22$ eV) emission line.

commensurate or incommensurate phases) may not be characteristic of adsorption on the more atomically rough (100) and (110) surfaces, on which one may expect a more strongly corrugated adsorbate-substrate potential. Evidence for the importance of this effect can be found in measurements and calculations of surface diffusion activation energies; for example, a recent calculation of this energy for diffusion of S on Ag, finds the value some $5 \times$ larger on Ag(100) than on Ag(111) [28]. In particular, a CsTCNQ₄ windmill phase is known to form on Ag(100) [29] but is commensurate; indeed, our own investigations of coadsorption phases of TCNQ with Na, K and Cs on Ag(100) have identified only commensurate phases [30,31]. The larger expected corrugation of the overlayer substrate interaction of this surface does appear to favour commensurate overlayer but this does not, of course, preclude the possibility that the cohesive energy within the salt layer exceeds the overlayer-substrate bonding energy.

Some insight into the changes in the electronic structure of the surface induced by these adsorption phases is provided by ultraviolet photoemission spectra (UPS) using incident He-I radiation (Fig. 4) and associated determinations of the surface work function by measuring the secondary electron emission cut-off (SECO) energy of UPS spectra recorded with a bias voltage of -10.00 V applied to the sample (Fig. S4). For TCNQ adsorbed on Ag(111), the UP spectrum clearly shows three peaks. By comparison with the calculated density of states for this phase [16], we identify the peaks at ~ 2.2 eV and ~ 0.9 eV to be the TCNQ HOMO and LUMO, with the latter becoming occupied upon adsorption. Upon coadsorption of alkali metals, these two peaks show significant shifts down in energy (to higher binding energy) and shift down further with increasing alkali coverage, indicating a strengthening of the interaction of the TCNQ with its surroundings. These shifts appear to be essentially independent of which alkali is incorporated into the layer, with the HOMO and LUMO states observed at ~ 2.3 eV and ~ 1.0 eV respectively for both windmill phases and ~ 2.6 eV and ~ 1.3 eV for both head-to-tail phases. By contrast, the work function changes (Table 2) do have a significant dependence on which alkali is present. As may be expected, adding the highly electropositive alkali atoms leads to significant decreases in the work function (which initially increases from its value for the clean surface following deposition of the electron acceptor TCNQ molecule). The larger decrease in work function induced by the CsTCNQ phase relative to that of the KTCNQ phase may be attributable to the fact that in these structures the Cs⁺ ions are higher above the surface than the K⁺ ions (see Fig. 2 and Table 1), leading to a larger dipole moment when combined with the image

Table 2
Work functions of the different Ag(111) surface phases investigated.

Surface phase	Work function (eV)
Clean Ag(111)	4.6
Ag(111)-TCNQ	5.0
Ag(111)-KTCNQ	4.4
Ag(111)-K ₂ TCNQ	3.9
Ag(111)-CsTCNQ	4.1
Ag(111)-Cs ₂ TCNQ	3.6

charge in the metal surface. Increasing the density of alkali ions in the overlayer to produce the K₂TCNQ and Cs₂TCNQ phases leads to a further decrease in the work function although its origin is less clear, as the detailed analysis of the charge transfer in K₂TCNQ [16] indicates most of the charge transfer is *within* the charge transfer salt layer, with very little transfer of electrons from the metal surface to the overlayer.

4. Conclusions

A comparison of our (previously published) structural characterisation of the coadsorption phases of TCNQ and K on Ag(111) with new results for the coadsorption phases of TCNQ and Cs on this surface shows very strong similarities indicating that the detailed structures and bonding character are largely independent of which alkali is incorporated. Of particular note is that this is true for both the K₂TCNQ and Cs₂TCNQ phases, which are, respectively, commensurate and incommensurate. This apparent insensitivity to commensuration is consistent with one key previous finding for the K₂TCNQ phase [16], namely, that the 2D charge transfer salt that is formed has a much stronger cohesive energy within the layer than the interaction with the underlying Ag(111) substrate. The extent to which this is also true for the KTCNQ and CsTCNQ phases is less clear. The fact that both these well-ordered overlayer phases are incommensurate clearly indicates that the cohesive energy within the layer is stronger than the lateral crystalline corrugation of overlayer-substrate interaction potential, but not necessarily than the average value of this potential.

CRedit authorship contribution statement

P.J. Blowey: Conceptualization, Data curation, Formal analysis, Investigation, Writing - original draft, Writing - review & editing. **L.A. Rochford:** Investigation, Writing - review & editing. **D.A. Duncan:** Investigation, Writing - review & editing. **P.T.P. Ryan:** Investigation, Writing - review & editing. **D.A. Warr:** Investigation, Writing - review & editing. **T.-L. Lee:** Investigation, Writing - review & editing. **G. Costantini:** Conceptualization, Writing - review & editing. **D.P. Woodruff:** Conceptualization, Data curation, Investigation, Writing - original draft, Writing - review & editing.

Declaration of Competing Interest

None

Acknowledgements

The authors thank Diamond Light Source for allocations SI15899 and NT18191 of beam time at beamline I09 that contributed to the results presented here. P.J.B. acknowledges financial support from Diamond Light Source and EPSRC. G.C. acknowledges financial support from the EU through the ERC Grant "VISUAL-MS" (Project ID: 308115).

Supplementary materials

Supplementary material associated with this article can be found, in

the online version, at doi:10.1016/j.susc.2020.121687.

References

- [1] D. Stradi, B. Borca, S. Barja, M. Garnica, C. Diaz, J.M. Rodriguez-Garcia, M. Alcamí, A.L. Vazquez de Parga, R. Miranda, F. Martin, RSC Adv. 6 (2016) 15071.
- [2] L. Romaner, G. Heimel, J.-L. Brédas, A. Gerlach, F. Schreiber, R.L. Johnson, J. Zegenhagen, S. Duhm, N. Koch, E. Zojer, Phys. Rev. Lett. 99 (2007) 256801.
- [3] T.-C. Tseng, C. Urban, Y. Wang, R. Otero, S.L. Tait, M. Alcamí, D. Écija, M. Trelka, J.M. Gallego, N. Lin, M. Konuma, U. Starke, A. Nefedov, A. Langner, C. Wöll, M. Á. Herranz, F. Martín, N. Martín, K. Kern, R. Miranda, Nat. Chem. 2 (2010) 374.
- [4] S. Barja, D. Stradi, B. Borca, M. Garnica, C. Díaz, J.M. Rodríguez-García, M. Alcamí, A.L.V. de Parga, F. Martín, R. Miranda, J. Phys. Condens. Matter. 25 (2013) 484007.
- [5] J.I. Martínez, E. Abad, F. Flores, J. Ortega, Phys. Status Solidi B 248 (2011) 2044.
- [6] M.N. Faraggi, N. Jiang, N. Gonzalez-Lakunza, A. Langner, S. Stepanow, K. Kern, A. Arnau, J. Phys. Chem. C 116 (2012) 24558.
- [7] A. Della Pia, M. Riello, D. Stassen, T.S. Jones, D. Bonifazi, A. De Vita, G. Costantini, Nanoscale 8 (2016) 19004.
- [8] P.J. Blowey, S. Velari, L.A. Rochford, D.A. Duncan, D.A. Warr, T.-L. Lee, A. De Vita, G. Costantini, D.P. Woodruff, Nanoscale 10 (2018) 14984.
- [9] I.G. Torrente, K.J. Franke, J.I. Pascual, Int. J. Mass. Spectrom. 277 (2008) 269.
- [10] M.M. Kamna, T.M. Graham, J.C. Love, P.S. Weiss, Surf. Sci. 419 (1998) 12.
- [11] C. Wäckerlin, C. Iacovita, D. Chylarecka, P. Fesser, T.A. Jung, N. Ballay, Chem. Commun. 47 (2011) 9146.
- [12] H. Yamane, N. Kosugi, J. Phys. Chem. Lett. 8 (2017) 5366.
- [13] A. Floris, A. Comisso, A. De Vita, ACS Nano 7 (2013) 8059.
- [14] D.P. Woodruff, Rep. Prog. Phys. 68 (2005) 743.
- [15] P.J. Blowey, L.A. Rochford, D.A. Duncan, D.A. Warr, T.-L. Lee, D.P. Woodruff, G. Costantini Faraday, Disc. 204 (2017) 97–110.
- [16] P.J. Blowey, B. Sohail, L.A. Rochford, T. Lafosse, D.A. Duncan, G. Costantini, R.J. Maurer, D. P. Woodruff, ACS Nano 14 (2020) 7475.
- [17] A. Haags, L.A. Rochford, J. Felter, P.J. Blowey, D.A. Duncan, D.P. Woodruff, C. Kumpf, N. J. Phys. 22 (2020) 063028.
- [18] D. Nečas, P. Klapetek, Cent. Eur. J. Phys. 10 (2012) 181–188.
- [19] C.J. Fisher, R. Ithrin, R.G. Jones, G.J. Jackson, D.P. Woodruff, B.C.C. Cowie, J. Phys. 10 (1998) L623.
- [20] M.B. Trzhaskovskaya, V.I. Nefedov, V.G. Yarzhevsky, At. Data Nucl. Data Tables 77 (2001) 97–159.
- [21] M. Konno, T. Ishii, Y. Saito, Acta Crystallogr. Sect. B 33 (1977) 763.
- [22] U. Schlickum, R. Decker, F. Klappenberger, G. Zoppellaro, S. Klyatskaya, M. Ruben, I. Silanes, A. Arnau, K. Kern, H. Brune, J.V. Barth, Nano Lett. 7 (2007) 3813.
- [23] Y. Geng, P. Li, J. Li, X. Zhang, Q. Zeng, C. Wang, Coord. Chem. Rev. 337 (2017) 145.
- [24] Y. Wang, S. Fabris, T.W. White, P. Moras, F. Pagliuca, M. Papagno, D. Topwal, P. Sheverdyeva, C. Carbonne, M. Lingenfelder, T. Classen, K. Kern, G. Costantini, Chem. Commun. 48 (2012) 534.
- [25] A. Haags, L.A. Rochford, J. Felter, P.J. Blowey, D.A. Duncan, D.P. Woodruff, C. Kumpf, N. J. Phys. 22 (2020) 063028.
- [26] C.J. Fritchie, Jr., P. Arthur, Jr., Acta Cryst. 21 (1966) 139.
- [27] H. Terauchi, Phys. Rev. B 17 (1978) 2446.
- [28] C.R.B. Rodriguez, J.A. Santana, J. Chem. Phys. 149 (2018) 204701.
- [29] N. Abdurakhmanova, A. Floris, T.-C. Tseng, A. Comisso, S. Stepanow, A. De Vita, K. Kern, Nat. Commun. 3 (2012) 940.
- [30] P.J. Blowey, PhD Thesis, University of Warwick, 2018.
- [31] P.J. Blowey et al., to be published.